Clinical Neurophysiology 125 (2014) 484–490

Contents lists available at ScienceDirect

Clinical Neurophysiology

journal homepage: www.elsevier.com/locate/clinph

Identifying electrode bridging from electrical distance distributions: A survey of publicly-available EEG data using a new method

Daniel M. Alschuler [a,*], Craig E. Tenke [a,b], Gerard E. Bruder [a,b], Jürgen Kayser [a,b]

[a] Division of Cognitive Neuroscience, New York State Psychiatric Institute, New York, NY, USA
[b] Department of Psychiatry, Columbia University College of Physicians & Surgeons, New York, NY, USA

ARTICLE INFO

Article history:
Accepted 25 August 2013
Available online 2 October 2013

Keywords:
Electroencephalogram (EEG)
Electrolyte bridge
Artifact
Electrical distance
Intrinsic Hjorth
Public dataset

HIGHLIGHTS

- An algorithm was developed to identify bridged electrodes using characteristics of electrical distance frequency distributions.
- Using this tool on five publically-available datasets, electrode bridges were detected in 54% of sessions.
- If used routinely, this automated approach offers feedback required to protect against spatial distortion and smoothing that might contaminate an EEG or ERP topography.

ABSTRACT

Objective: EEG topographies may be distorted by electrode bridges, typically caused by electrolyte spreading between adjacent electrodes. We therefore sought to determine the prevalence of electrode bridging and its potential impact on the EEG literature.
Methods: Five publicly-available EEG datasets were evaluated for evidence of bridging using a new screening method that employs the temporal variance of pairwise difference waveforms (electrical distance). Distinctive characteristics of electrical distance frequency distributions were used to develop an algorithm to identify electrode bridges in datasets with different montages (22–64 channels) and noise properties.
Results: The extent of bridging varied substantially across datasets: 54% of EEG recording sessions contained an electrode bridge, and the mean percentage of bridged electrodes in a montage was as high as 18% in one of the datasets. Furthermore, over 40% of the recording channels were bridged in 9 of 203 sessions. These findings were independently validated by visual inspection.
Conclusions: The new algorithm conveniently, efficiently, and reliably identified electrode bridges across different datasets and recording conditions. Electrode bridging may constitute a substantial problem for some datasets.
Significance: Given the extent of the electrode bridging across datasets, this problem may be more widespread than commonly thought. However, when used as an automatic screening routine, the new algorithm will prevent pitfalls stemming from unrecognized electrode bridges.

1. Introduction

Topographic analyses of scalp EEG measures rely on accurate spatial localization of the surface potentials recorded at each electrode (e.g., Junghöfer et al., 1997). In most EEG studies, electrode contact with the scalp is established via an electrolyte gel or solution. The incidental spread of this electrolyte can cause low-impedance electrical bridges between two or more electrodes (Tenke and Kayser, 2001), as well as introduce marked variability into the effective size of each scalp recording site (Greischar et al., 2004). These problems may be further exacerbated for some participants by perspiration, particularly in warm environments (Kappenman and Luck, 2010). Channels can also be bridged via less obvious mechanisms, such as physical damage to wires, plugs, or jumpers. Regardless of their cause, electrical bridges result in spuriously identical, or almost identical, EEG signals at each sensor spanned by a given bridge. Although rarely acknowledged in the

* Corresponding author. Address: New York State Psychiatric Institute, Division of Cognitive Neuroscience, Unit 50, 1051 Riverside Drive, New York, NY 10032, USA. Tel.: +1 212 543 5466.
E-mail address: alschul@nyspi.columbia.edu (D.M. Alschuler).

1388-2457/$36.00
http://dx.doi.org/10.1016/j.clinph.2013.08.024

literature, such bridges have the potential to severely distort or spatially smooth an EEG or ERP topography, confounding conventional descriptions and inferences while invalidating source localization estimates (Tenke and Kayser, 2001; Greischar et al., 2004).

Electrical bridging is not readily apparent when viewing continuous, epoched, or averaged data, even for a limited number of EEG channels (e.g., 32 or less; Fig. 1). The only reliable methods in the literature for finding bridged electrodes rely on pairwise comparisons between channels to find those whose signals are nearly identical. This can be accomplished by graphically superimposing two EEG/ERP waveforms (cf. Fig. 1). However, this requires considerable scrutiny and diligence on the part of the researcher as well as the willingness to invest the considerable extra time, especially as the number of channels increases (i.e., up to 256 or more). Unsystematic inspections using this approach, while faster and easier, may miss bridged electrodes. However, a direct visual comparison can be replaced by a systematic numerical approach based on the temporal variance of pairwise differences between waveforms recorded at each electrode in a montage. The resulting electrical distance (ED) measure may then be applied to facilitate the visual identification of bridges (e.g., intrinsic Hjorth algorithm; Tenke and Kayser, 2001).

The complete set of EDs computed from all epochs of an EEG recording session provides an informative summary of the similarity or dissimilarity of waveforms in the montage. Kayser and Tenke (2006) outlined an artifact rejection method based on the set of channel × channel ED matrices of every trial in an epoched recording. This approach employs the ED measure as an index of similarity: surface potentials obtained at neighboring sites can be expected to be quite similar due to volume conduction. ED fre-

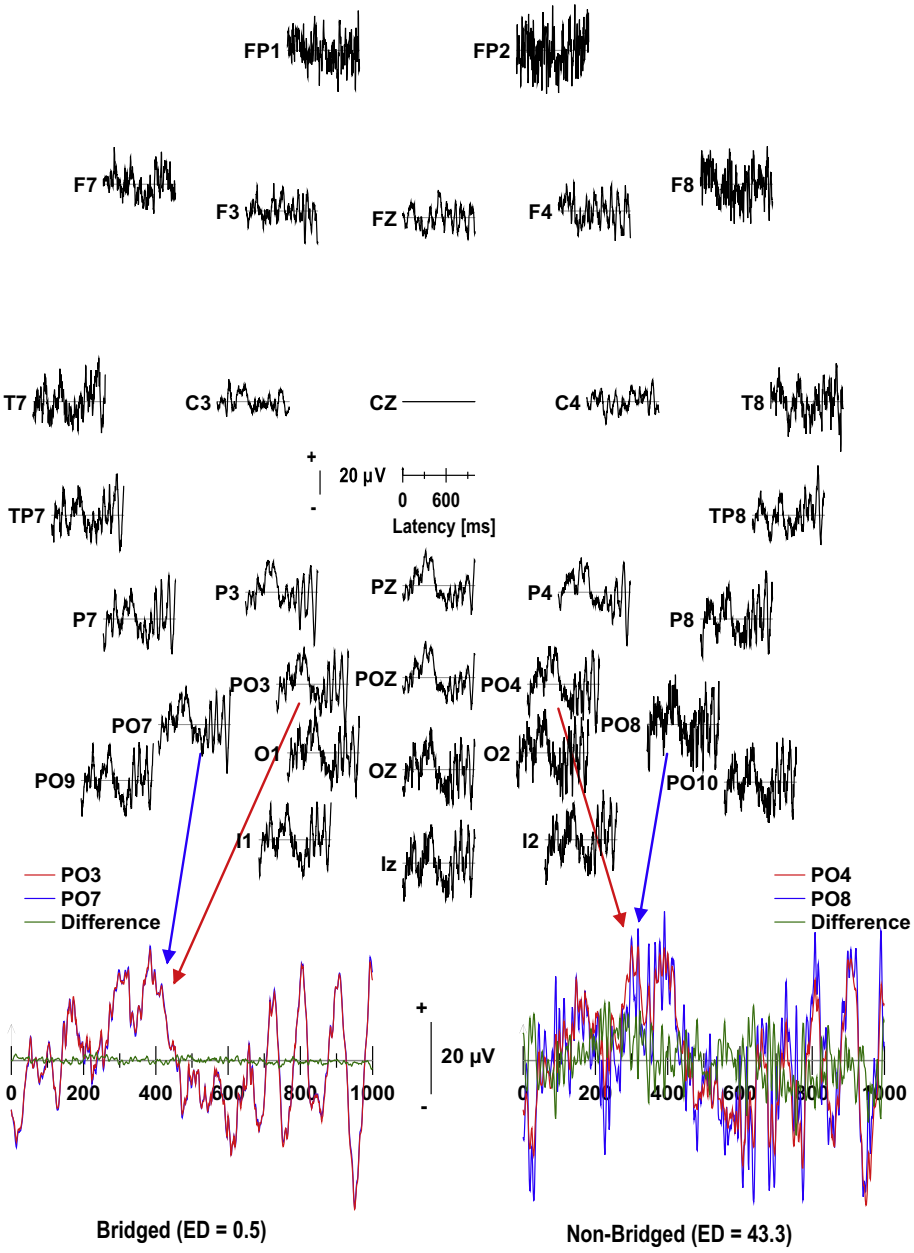

Fig. 1. A single sweep from dataset A_{32} with 6 bridged electrodes (6/32 channels: PO3, PO7, IZ, I1, I2, PO9). Data were minimally processed (1-s epochs, baselined, with added Cz reference channel). Enlarged, superimposed waveforms exemplify a bridged (PO3/PO7) and a non-bridged (PO4/PO8) pair of adjacent channels. The corresponding difference waveforms, along with their respective EDs, quantify the degree of similarity, which can in turn be used to operationalize electrode bridging. Note that, without foreknowledge of which channels were bridged, finding electrode bridges without any sort of pairwise channel-by-channel comparison would be extremely difficult.

quency distributions are used to identify epoch-by-epoch channel pairs that have high dissimilarity (i.e., an unusually large ED), therefore suggesting an underlying artifact (of undetermined cause). The same approach can also be applied to use the expected characteristics of frequency distributions of epoch-by-epoch EDs to identify extremely small EDs, which should characterize bridged electrodes.

Although the problem of electrode bridging has been tacitly acknowledged (e.g., Luck, 2005), the prevalence of electrode bridging in the datasets contributing to the literature is unknown. Moreover, differences between recording montages or noise properties of recording systems will affect the scale and properties of a set of difference waveforms and their associated EDs, rendering the visual identification of bridged electrodes even more difficult when applied across multiple recording systems. The availability of an objective, automated detection method (i.e., a method that is not affected by differences between acquisition systems, equipment- or site-specific noise properties, and different recording montages) would enable the quantification of this problem across EEG data collected in different laboratories. The objective of this study was therefore to identify and employ publically-available EEG datasets to create, test and refine a new algorithm that exploits characteristics of ED frequency distributions, permitting a quantitative evaluation of electrode bridging both in each dataset and across datasets.

2. Methods

2.1. Electrical distance and bridge detection

A potential difference waveform is defined as the difference between the time-varying potentials P of channels i and j, computed as:

$$P_{i-j}(t) = P_i(t) - P_j(t)$$

Because any two channels that are electrically bridged will have near-identical waveforms, bridged channels can be identified as those pairs with low-amplitude difference waveforms. The overall amplitude of a difference waveform can be quantified by its variance over time T (temporal variance; Tenke and Kayser, 2001), defined as:

$$ED_{i-j} = \frac{1}{T}\sum_{t=1}^{T}\left(P_{i-j}(t) - \overline{P_{i-j}(t)}\right)^2$$

The ED measure was originally implemented in NeuroScan 3.0 (Neuroscan Inc., 1993, 1995) as an electrical analogue of distance for a Hjorth Laplacian montage ("intrinsic Hjorth"; cf. footnote 2 in Tenke and Kayser, 2001), yielding topographies sharpened over electrical, rather than spatial, distance. The intrinsic Hjorth identifies electrical bridges in averaged waveforms as flat (i.e., near-zero ED) waveforms for bridged channels (cf. Fig. 1 in Tenke and Kayser, 2001). This approach has been successfully applied in numerous research studies (e.g., Greischar et al., 2004; Tenke et al., 2008; Knight et al., 2010; Hamm et al., 2012; Kayser et al., 2012) and commercial software products (e.g., Electrical Geodesics Inc., 2003) to identify and address problems stemming from bridged recording channels[1].

[1] While the intrinsic Hjorth beta feature has been abandoned in more recent releases of NeuroScan software, the implications of Tenke and Kayser (2001) were recognized as a potential problem, prompting Electrical Geodesics, Inc. to incorporate an electrical distance analog into their Netstation software at the time (Electrical Geodesics Inc., 2003). Additional nuances of the problem were identified shortly after by Greischar et al. (2004), but there have been no further developments since then. When our research group recently became responsible for the oversight and analysis of EEG/ERP data at multiple test sites, each of which used different equipment, we decided to establish a common, standardized approach to address this issue.

2.2. EEG data

Sets of EEG recordings were obtained via an Internet search restricted to those freely available for direct download or upon request. Datasets were used if: (1) they were associated with a publication; (2) the EEG montage consisted of at least 20 channels; and (3) at least 15 sessions were available. A session was defined as an individual time period during which an electrode cap was applied and EEG data were acquired for at least 50 s. Five datasets, some of which were used in more than one publication, met these selection criteria and were accordingly used for this survey (BCI2000; Goldberger et al., 2000; Delorme et al., 2002, 2004; Delorme and Makeig, 2004; Schalk et al., 2004; Naeem et al., 2006; Savran et al., 2006; Koelstra et al., 2012). These datasets were randomly labeled A–E, with a subscript to indicate the number of channels in the montage (Table 1). Three sessions were excluded from the analyses due to flat EEG, amplifier saturation, or non-physiological artifacts. Sets A_{32} (100 Hz low-pass, 50 Hz notch), B_{64} (0.1 Hz high-pass, 60 Hz low-pass) and C_{22} (0.5–50 Hz band-pass, 50 Hz notch) had already been filtered at the acquisition sites. Data were acquired using a variety of reference schemes, including acquisition- or system-specific references, but all sessions were re-referenced to vertex (Cz) during preprocessing. However, it should be noted that EDs are computed from pairwise difference waveforms and that any approach that utilizes EDs is therefore inherently reference-free and unaffected by the choice of EEG reference.

2.3. Preprocessing

All data from a given session were imported into MATLAB R2010a (The MathWorks, Inc., 2010; with Signal Processing Toolbox v6.13) using EEGLAB v11.0.3.1b (Delorme and Makeig, 2004; Vidaurre et al., 2011). The EEG data from some of the sessions were stored in multiple files; in these cases, the data from a given session were merged into a single data structure using the EEGLAB pop_mergeset.m function. For three sessions in B_{64}, the first two files out of 14 were recorded at a different sample rate than the other twelve files in each of those sessions and were therefore discarded. Cz was the only recording site commonly used as a reference channel to appear in all 5 montages and was accordingly chosen as the reference for all data. All data using a different reference were thus re-referenced to Cz using the EEGLAB pop_reref.m function. All channels corresponding to recording sites that were not an integral part of an electrode cap (e.g., Nose, EOG) were removed with a custom MATLAB script. The data were then resampled to 128 samples/s using the pop_resample.m function, and FIR 0.5 Hz high-pass and 30 Hz low-pass filters were applied using the "fir1" option of the EEGLAB pop_eegfilt.m function. This filtering was intended to remove any high- and low-frequency noise that might differentially affect the signal variance (i.e., EDs) across datasets. Informal observations of both continuous data and FFT frequency averages indicated that this filter did not cause any noticeable distortion of the data. Finally, the continuous data were transformed into consecutive 1-s epochs (128 samples) using a

Table 1
Core characteristics of EEG data included in current study.

$Dataset_{Number\ of\ channels}$	A_{32}	B_{64}	C_{22}	D_{32}	E_{54}
Number of subjects	16	109	9	32	5
Sessions per subject	2	1	2	1	3
Total sessions	31[a]	109[b]	18	32	13[b]

[a] 1 out of 32 sessions excluded.
[b] 2 out of 15 sessions excluded.

custom MATLAB script. This epoch length was long enough to provide sufficient samples to compute epoch-by-epoch EDs, but short enough to permit a satisfactory number of epochs to be extracted from each recording.

2.4. Implementation

Following the approach of Kayser and Tenke (2006), the epoched data began as a channels × epochs × sample points MATLAB matrix. A channels × channels × epochs ED matrix was then computed from the epoched data, and each ED value in the matrix was multiplied by a scale factor (100/median ED value). The set of EDs was summarized by its frequency distribution (bin size = 0.25) and, in order to improve reliability and resolution, the distribution was interpolated to a bin size of .05 (cubic spline interpolation). Upon inspection, many of the interpolated frequency distributions were found to exhibit a near-zero local peak (Fig. 2). All of these local peaks occurred at an ED $\leqslant$ 5, and the local minima that followed these peaks all occurred at an ED $\leqslant$ 10. Validation against the intrinsic Hjorth algorithm showed that this local peak was confined almost exclusively to sessions with bridging. We therefore concluded that these near-zero peaks accurately represent the extremely low EDs of bridged pairs of channels.

A formal algorithm was accordingly developed from these observations (Fig. 3). The algorithm first creates an ED frequency distribution and then determines the presence of a near-zero local peak. If no such peak exists, no channels are flagged as bridged. If a peak exists, the local minimum with an ED $\leqslant$ 10 following the peak is automatically identified and set as the ED cutoff. If 50% or more of all epochs for any given pair of channels are less than or equal to this ED cutoff, both channels are classified as bridged. This algorithm was applied to all EEG recording sessions (the Matlab code for the algorithm and the necessary preprocessing can be obtained at http://psychophysiology.cpmc.columbia.edu/eBridge).

2.5. Recording and segmenting parameters

To test the effects of changes to various data parameters on the performance of the algorithm, the sample rate, number of epochs, and epoch length from each session were altered systematically. The sample rate was varied by resampling the continuous data from 128 to 64 samples/s using the EEGLAB pop_resample.m function and then epoching the data (as described above). The number of epochs was varied by semi-randomly choosing 30, 120, or 480 epochs in comparison to the initial number of epochs in all sessions (>960). Epoch length was varied by epoching the continuous data from each session into 0.5-, 1- or 2-s epochs and then semi-randomly choosing 480 epochs to control for number of epochs.

The algorithm was then applied to every session in the sample of public datasets, for each sample rate, number of epochs, and epoch length. The channels labeled by the algorithm as bridged or not bridged were compared to a benchmark produced from the original preprocessed data (128 samples/s, all epochs included, 1-s epochs). A similarity index was then computed for every session and comparison, defined as the sum of channels flagged as bridged or not bridged in both the benchmark and the comparison data, divided by the total number of channels in the montage and multiplied by 100. An index of 100 therefore indicates complete agreement in flagged channels between the benchmark and comparison data (maximum similarity) whereas an index of 0 indicates total disagreement (maximum dissimilarity).

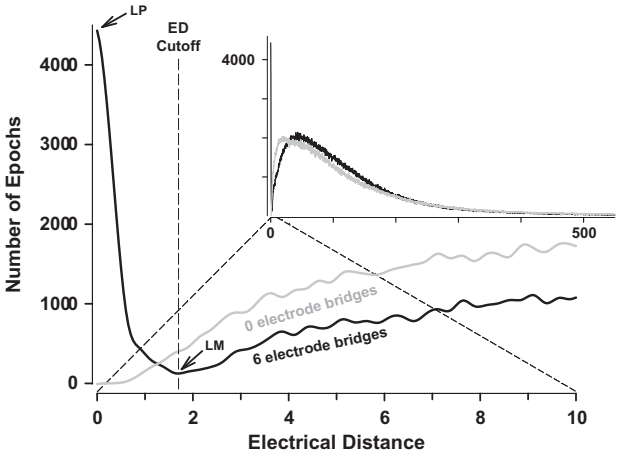

Fig. 2. Spline-interpolated partial frequency distributions of electrical distances from two sessions of dataset A_{32}, one with 6 bridged electrodes (same session as used in Fig. 1) and one with no bridged electrodes. The number of epochs are plotted as a function of electrical distance (the inset shows almost the entire frequency distributions of the electrical distances). For the session with bridging, the ED cutoff is defined as the local minimum (LM) with an ED $\leqslant$ 10 and following the first local peak (LP). Note that the near-zero local peak only occurs in the session with bridging, presumably because of a high number of epochs with low EDs due to bridged channels.

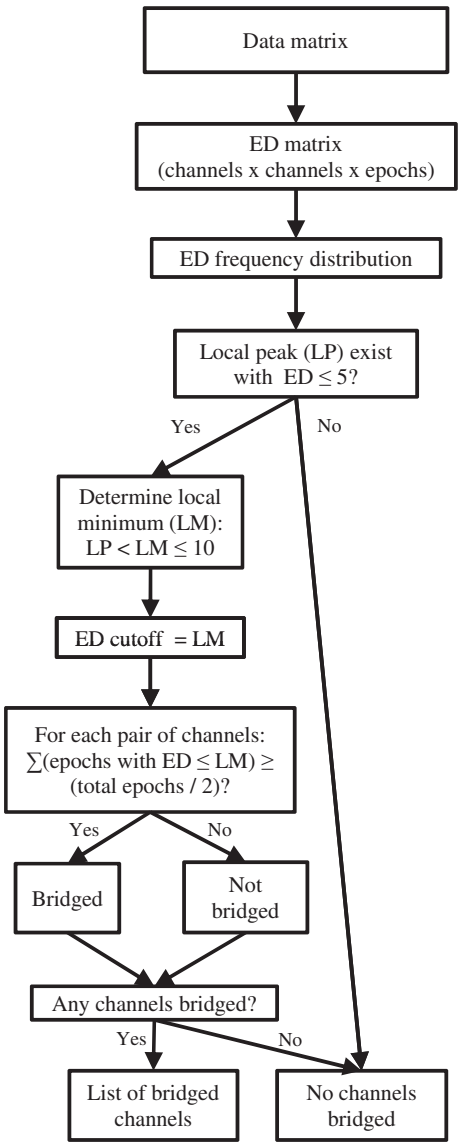

Fig. 3. Flowchart overview of algorithm for detecting electrical bridging.

2.6. Tests with unprocessed data

To ensure that the apparent electrode bridges found by the algorithm were not related to the preprocessing procedures, the raw data (i.e., the data as originally downloaded) were: 1 imported into EEGLAB and: (1) not filtered; (2) low-pass filtered; or (3) band-pass filtered (filters described above). The three resulting lists of bridged channels were then compared to a benchmark list produced from the original preprocessed data and similarity indices were calculated as described above.

2.7. Simulation of an electrode bridge

A single, preprocessed session from dataset A_{32} without any bridged electrodes was selected (cf. Fig. 2; the lack of bridged channels was confirmed via intrinsic Hjorth). For each data point in channel C3, a weighted average was calculated with the corresponding point in P3 (e.g., 50% for each channel would yield an arithmetic mean). The corresponding computation was performed for each data point in P3. The degree of similarity between the two EEG channels was systematically varied by repeating this process with weightings that varied in increments of 10% between 100% and 60% (0% and 40% for the second channel), and in increments of 1% between 59% and 50% (41% and 50% for the second channel).

3. Results

3.1. Algorithm validation

The ED cutoffs for all sessions were validated by visual inspection of the ED distributions, noting the location of the cutoff along the abcissa. In all cases, the ED cutoffs were placed at, or in close proximity to, the local minimum. Validation against the intrinsic Hjorth algorithm indicated a close agreement between the sets of channels labeled as bridged by the two methods.

The ED frequency distributions from several sessions were divided to separate those identifying bridged electrode pairs from EDs that did not (Fig. 4). In each of these sessions, the bridged and non-bridged distributions were unambiguously separated: the bridged distribution accounted for the near-zero peak in the main distribution, whereas the non-bridged distribution accounted for the remainder.

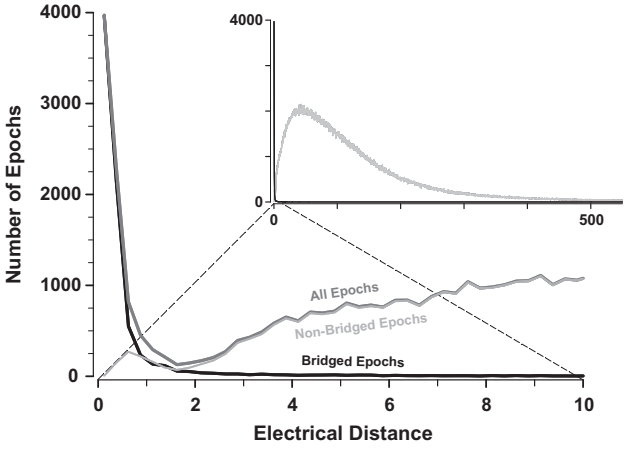

Fig. 4. Electrical distance frequency distributions (not spline-interpolated) separately plotted for epochs from bridged and non-bridged electrode pairs (plotting and inset as in Fig. 2; distributions only include data from the session with 6 bridged electrodes used in Figs. 1 and 2). Note that the near-zero local peak only occurs in the distribution of epochs from bridged electrode pairs.

3.2. Total electrode bridging in datasets

Electrode bridging (percentage of sessions with any bridging; mean percentage of bridged electrodes in the montage) was detected in datasets A_{32} (87%; 18%), B_{64} (75%; 10%), and E_{54} (8%; 0.3%) (Table 2). More than 40% of channels were flagged as bridged in a total of 9 sessions (5 from A_{32} and 4 from B_{64}). As stated above, these findings were not just a product of the developed algorithm, but were verified by direct visual inspection and application of the intrinsic Hjorth.

3.3. Recording, segmenting, and processing parameter comparisons

Table 3 lists the mean similarity indices resulting from the different data recording, segmenting, and processing methods in comparison to the original benchmark bridging analysis. All comparisons showed overwhelming similarity ($\geqslant$98.7), although the corresponding SDs varied notably.

3.4. Simulation of an electrode bridge

The simulated bridge between two channels (C3 = P3; 50% weighting for each) was correctly identified. The algorithm only identified nonidentical waveforms as bridged when the difference from this simulated bridge was extremely small (<3%; cf. Fig. 5).

4. Discussion

The bridge-detection method described here provides an objective and efficient means for reliably detecting electrode bridges in continuous EEG recordings. The algorithm exploits characteristic features of a frequency distribution of electrical distance values that are only present if two or more channels are bridged. It can be easily implemented and appears to yield near-identical findings when compared with direct visual inspection or intrinsic Hjorth. Given that the algorithm yields comparable results when applied to the original datasets, some of which were completely unprocessed, the preprocessing methods do not seem to inflate the incidence of detected electrode bridges. Furthermore, the algorithm gives reliable results even across different recording methods and segmenting parameters. Because the underlying ED measure is based on pairwise difference waveforms between any two recording sites, the algorithm does not depend on the EEG recording reference (for a discussion of the effects of reference choice on surface potentials, see Kayser and Tenke, 2010). The algorithm is therefore suitable as a generic tool to verify a critical aspect of EEG data integrity.

Electrode bridging varied significantly between datasets. It is unclear if certain acquisition parameters or specific recording characteristics are more likely to result in electrode bridges (e.g., EEG recording equipment, number and proximity of recording sites, hair properties, technician skills, etc.). Although these questions are beyond the scope of this report, it should be noted that the greatest montage density in this report consisted of only 64 electrodes. Findings by Greischar et al. (2004) and Tenke and Kayser (2001) suggest that most bridging is probably due to the spreading of electrolyte along the scalp to adjacent electrodes. The use of high-density montages (128 or more scalp locations), with correspondingly smaller inter-electrode distances, may therefore increase the incidence of electrical bridging. However, this is an empirical issue and could be laid to rest by applying the proposed algorithm to EEG data acquired from montages of various densities.

The algorithm used in this report may be overly conservative, as a few sessions were found with frequency distributions that featured not only a near-zero peak but also a second peak with an

Table 2
Electrode bridging by dataset.

Dataset	A_{32}	B_{64}	C_{22}	D_{32}	E_{54}	Sum
Total number of sessions	31	109	18	32	13	203
Number of sessions with at least one pair of bridged electrodes (%)	27 (87)	82 (75)	0 (0)	0 (0)	1 (8)	110 (54)
Mean percentage of bridged electrodes in EEG montage	18	10	0	0	0.3	8

Table 3
Similarity of identified bridges after varying recording and segmenting parameters.

Comparison to benchmark	Similarity index	
	Mean	SD
Sample rate (samples/s)		
64	99.9	1.18
Number of epochs		
30	99.0	3.84
120	99.6	2.31
480	99.8	1.24
Epoch length (seconds)		
0.5	99.8	1.30
1	99.8	1.24
2	99.7	1.62
Raw data		
Unfiltered	98.7	6.86
Low-pass	99.7	1.53
Band-pass	100.0	0.24

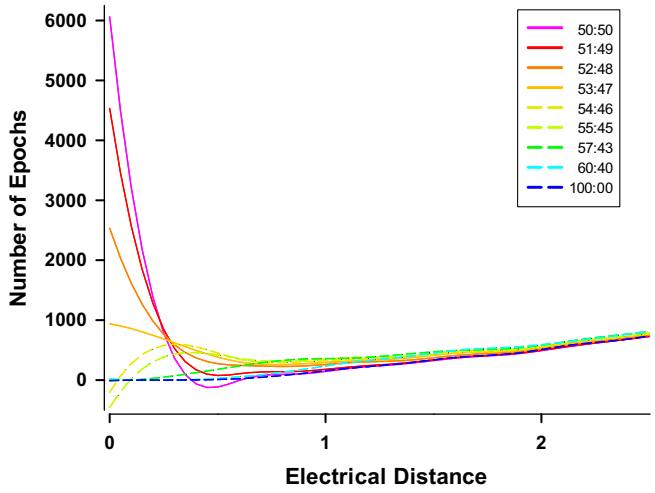

Fig. 5. Simulated electrode bridge: spline-interpolated electrical distance frequency distributions as a function of EEG waveform similarity using data from a session without bridging (same session as used in Fig. 2). Each distribution is from a copy of the session with P3 and C3 replaced by weighted averages of the two channels (percentage of original channel: percentage of other channel). C3 and P3 were flagged as bridged by the new algorithm only for the 50:50%, 51:49%, 52:48%, and 53:47% weightings (solid lines).

ED $\leqslant$ 10. Although formal analyses of these second peaks were not performed, these peaks may reflect additional electrodes with a more tenuous electrical bridge (i.e., electrodes with a strong electrical bridge form the first peak and electrodes that are more weakly or variably bridged together form the second peak). Ignoring these second peaks may therefore risk some lesser distortion of EEG topographies, but further research is needed to address this issue.

Our evaluation of the bridge detection algorithm with publicly-available datasets strongly suggests that it may be readily applied to EEG acquired with any recording system. Given the unexpected prevalence of bridging detected across the samples selected for this study, it is likely that bridging represents a pervasive problem in data contributing to the EEG literature. This high incidence is counterintuitive for any published dataset, and underscores a problem that is largely unrecognized by the field. Rather than risk the noise that results from unnecessarily high scalp impedances, many experimenters will over-apply electrolyte. This practice is reinforced when the resulting data (i.e., individual waveforms) are of sufficient quality to yield publishable averages. In contrast, electrode bridging is nearly impossible to intuitively recognize in continuous, epoched, or averaged data, even with close inspection (e.g., Fig. 1). Unfortunately, undetected bridged electrodes degrade the quality and precision of an EEG topography in a way that counters the trend toward higher density montages. In fact, variability in the size and consistency of the electrolyte interface may itself have topographic implications, even in the absence of identified bridges (Greischar et al., 2004). On the other hand, the prevalence of electrode bridges in low-density montages may constitute an even greater distortion of the EEG topography.

The proposed approach thereby provides an essential tool to help recover the topographic precision of data to a caliber required for the extrapolation to dural or intracranial neuronal generator patterns, or even scalp surface Laplacian (current source density) techniques (e.g., Tenke and Kayser, 2012). It is therefore recommended that systematic screening for electrode bridging become a standard part of any EEG data analysis, for example, as regular a practice as the detection (and reduction) of blink artifacts. Such a safeguard would allow informed decisions to be made about how to address any bridging. Affected data can be excluded (trials, time interval, subjects) or replaced (e.g., interpolation), thereby avoiding potential distortions of the data or other pitfalls. Even if no electrode bridges were present in a given dataset, a routine screening would provide certainty of their absence and thereby allow for greater confidence in any topographic analyses.

Acknowledgements

This work was supported in part by Grants MH36295 and MH092250 from the National Institute of Mental Health (NIMH). Preliminary analyses of these data were presented at the 52nd Annual Meeting of the *Society for Psychophysiological Research (SPR)*, New Orleans, LA, September 19–23, 2012. Waveform plotting software was provided by Charles L. Brown, III. The authors would like to acknowledge Mark Pflieger for developing the original intrinsic Hjorth routine. We appreciate the helpful comments from two anonymous reviewers.

References

BCI2000 (n.d.). Retrieved from <http://www.bci2000.org>.
Delorme A, Makeig S. EEGLAB: an open source toolbox for analysis of single-trial EEG dynamics including independent component analysis. J Neurosci Methods 2004;134:9–21.
Delorme A, Makeig S, Fabre-Thorpe M, Sejnowski T. From single-trial EEG to brain area dynamics. Neurocomputing 2002;44–46:1057–64.
Delorme A, Rousselet GA, Mace MJ, Fabre-Thorpe M. Interaction of top–down and bottom-up processing in the fast visual analysis of natural scenes. Cogn Brain Res 2004;19:103–13.
Electrical Geodesics, Inc. On-line detection of electrolyte bridges. EGI Newsletter 2003;7:1.

Goldberger AL, Amaral LA, Glass L, Hausdorff JM, Ivanov PC, Mark RG, et al. PhysioBank, PhysioToolkit, and PhysioNet: components of a new research resource for complex physiologic signals. Circulation 2000;101:E215–220.
Greischar LL, Burghy CA, van Reekum CM, Jackson DC, Pizzagalli DA, Mueller C, et al. Effects of electrode density and electrolyte spreading in dense array electroencephalographic recording. Clin Neurophysiol 2004;115:710–20.
Hamm JP, Dyckman KA, McDowell JE, Clementz BA. Pre-cue fronto-occipital alpha phase and distributed cortical oscillations predict failures of cognitive control. J Neurosci 2012;32:7034–41.
Junghöfer M, Elbert T, Leiderer P, Berg P, Rockstroh B. Mapping EEG-potentials on the surface of the brain: a strategy for uncovering cortical sources. Brain Topogr 1997;9:203–17.
Kappenman ES, Luck SJ. The effects of electrode impedance on data quality and statistical significance in ERP recordings. Psychophysiology 2010;47:888–904.
Kayser J, Tenke CE. Electrical distance as a reference-free measure for identifying artifacts in multichannel electroencephalogram (EEG) recordings. Psychophysiology 2006;43:S51.
Kayser J, Tenke CE. In search of the Rosetta Stone for scalp EEG: converging on reference-free techniques. Clin Neurophysiol 2010;121:1973–5.
Kayser J, Tenke CE, Kroppmann CJ, Alschuler DM, Fekri S, Gil R, et al. A neurophysiological deficit in early visual processing in schizophrenia patients with auditory hallucinations. Psychophysiology 2012;49:1168–78.
Knight JB, Ethridge LE, Marsh RL, Clementz BA. Neural correlates of attentional and mnemonic processing in event-based prospective memory. Front Hum Neurosci 2010;4:5.
Koelstra S, Mühl C, Soleymani M, Lee JS, Yazdani A, Ebrahimi T, et al. DEAP: a database for emotion analysis using physiological signals. IEEE Trans Affect Comput 2012;3:18–31.
Luck SJ. An introduction to the event-related potential technique. Cambridge, MA: The MIT Press; 2005. p. 122.
Naeem M, Brunner C, Leeb R, Graimann B, Pfurtscheller G. Seperability of four-class motor imagery data using independent components analysis. J Neural Eng 2006;3:208–16.
Neuroscan Inc. SCAN Manual II Version 3.0. Herndon, VA; 1993.
Neuroscan Inc. Intrinsic Hjorth transform. SCAN 3.0 technical note. Herndon, VA; 1995.
Savran A, Ciftci K, Chanel G, Mota JC, Viet LH, Sankur B, et al. Emotion detection in the loop from brain signals and facial images. Presented at eNTERFACE'06, Dubrovnik, Croatia; 2006.
Schalk G, McFarland DJ, Hinterberger T, Birbaumer N, Wolpaw JR. BCI2000: a general-purpose brain-computer interface (BCI) system. IEEE Trans Biomed Eng 2004;51:1034–43.
Tenke CE, Kayser J. A convenient method for detecting electrolyte bridges in multichannel electroencephalogram and event-related potential recordings. Clin Neurophysiol 2001;112:545–50.
Tenke CE, Kayser J. Generator localization by current source density (CSD): implications of volume conduction and field closure at intracranial and scalp resolutions. Clin Neurophysiol 2012;123:2328–45.
Tenke CE, Kayser J, Shankman SA, Griggs CB, Leite P, Stewart JW, et al. Hemispatial PCA dissociates temporal from parietal ERP generator patterns: CSD components in healthy adults and depressed patients during a dichotic oddball task. Int J Psychophysiol 2008;67:1–16.
The MathWorks, Inc.. MATLAB and Statistics Toolbox Release 2010a. Natick, MA: The MathWorks, Inc.; 2010.
Vidaurre C, Sander TH, Schlogl A. BioSig: the free and open source software library for biomedical signal processing. Comput Intell Neurosci 2011;2011:935364.